ECS Journal of Solid State Science and Technology

Structural and Magnetic Studies on Iron Oxide and Iron-Magnesium Oxide Thin Films Deposited Using Ferrocene and (Dimethylaminomethyl)ferrocene Precursors

To cite this article: Kaupo Kukli *et al* 2013 *ECS J. Solid State Sci. Technol.* **2** N45

ECS Journal of Solid State Science and Technology, **2** (3) N45-N54 (2013)
2162-8769/2013/2(3)/N45/10/$28.00 © The Electrochemical Society

Structural and Magnetic Studies on Iron Oxide and Iron-Magnesium Oxide Thin Films Deposited Using Ferrocene and (Dimethylaminomethyl)ferrocene Precursors

Kaupo Kukli,[a,b,z] Mukesh Chandra Dimri,[c] Aile Tamm,[b] Marianna Kemell,[a] Tanel Käämbre,[b] Marko Vehkamäki,[a,*] Manjunath Puttaswamy,[a] Raivo Stern,[c] Ivar Kuusik,[b] Arvo Kikas,[b] Massimo Tallarida,[d] Dieter Schmeißer,[d] Mikko Ritala,[a,*] and Markku Leskelä[a]

[a] *University of Helsinki, Department of Chemistry, University of Helsinki, FI-00014 Helsinki, Finland*
[b] *University of Tartu, Institute of Physics, Department of Materials Science, EE-51014 Tartu, Estonia*
[c] *National Institute of Chemical Physics and Biophysics, EE-12618 Tallinn, Estonia*
[d] *Department of Physics, Brandenburg University of Technology, D-03046 Cottbus, Germany*

Iron oxide and magnesium-doped iron oxide films were grown by atomic layer deposition in the temperature range of 350–500°C from ferrocene, (dimethylaminomethyl)ferrocene, magnesium β-diketonate, and ozone. Phase composition of the films depended on the deposition temperature, as magnetite and/or maghemite tended to form instead of hematite upon lowering the temperature. Iron oxide layers were also mixed with magnesium oxide by alternate deposition of MgO and Fe_2O_3 which also favored the formation of magnetite or maghemite structure prior to hematite. Scanning electron microscopy implied the smoothening of the films after doping with magnesium oxide. Magnetometry was used to study the effects of temperature and doping levels on the magnetic properties of the films.
 [DOI: 10.1149/2.004303jss]

Manuscript submitted September 17, 2012; revised manuscript received December 3, 2012. Published December 20, 2012.

Iron oxide films have gained substantial interest as materials with potential applications in micro- and nanodevices. Hematite (α-Fe_2O_3) films can be used as solar cell[1] or gas sensor[2] materials. Iron oxide may also be used for the improvement of oxygen conversion ability of zirconia-based solid oxide fuel cells.[3] Magnetite (Fe_3O_4, $FeFe_2O_4$) films can be regarded as transparent magnetic, half-metallic, and conductive oxides,[4,5] which can also demonstrate magnetoresistance,[6] i.e the property of an interest in the field of magnetic sensors and data storage.

Iron oxide has been combined with other materials, in particular with MgO, in order to modify the properties of the material and, potentially, create magnetic device prototypes. For instance, magneto-optical behavior of ferrimagnetic γ-Fe_2O_3 (maghemite) films on MgO has been studied.[7] Fe_3O_4 has been described as a ferrite with lattice constant approximately twice as large as that of MgO,[8] referring to the possibility to realize substrate-oriented growth and structurally matched interfaces. Fe_3O_4-based spin valve stacks have been fabricated with MgO tunnel dielectrics.[9–11] Epitaxy of γ-Fe_2O_3, i.e. another structurally well-defined iron oxide on MgO has also been reported.[12] In addition, MgO has been used as a base material for nanopatterned structures,[13] possibly aiming at the further development of patterned magnetic media. It is worth noting, that the useful effects of magnesium oxide are not limited to magnetic properties. For instance, Mg-doped Fe_2O_3 can be used in photovoltaics as Mg-doped iron (III) oxide thin film electrodes that exhibit p-type behavior and can be synthesized by a pyrolytic method.[14] Ternary $MgFe_2O_4$, i.e. the magnesioferrite, could be applied as humidity sensor.[15] It appears, therefore, quite interesting to study the effect of MgO on the growth of iron oxide phases.

It has been known for a long time that bulk magnetite gives more than 200 times higher saturation magnetization values at room temperature, than hematite.[16] Maghemite and magnetite films have typically demonstrated higher saturation magnetization values, compared to hematite films.[17] Magnetization of films containing phase mixture can thus be still higher than that of hematite films. It has also been reported that even amorphous films consisting of Fe_3O_4 can demonstrate saturation magnetization, although the coercivity was hardly detectable.[18] Also maghemite films laser ablated on MgO substrates have demonstrated saturation magnetization approximately ten times higher than hematite films.[19] Magnesioferrites have been synthesized, e.g. by sol-gel and measured earlier,[20] and ferromagnetic behavior has been observed in such materials, too.[21,22] Therefore, one cannot conclude on the formation of magnetite in the thin films such as those grown in the present study only on the basis of the magnetometric results. Moreover, in the case of nanodimensional films, i.e. materials containing nanocrystallites, one should not exclude the appearance of magnetization due to the defective structures characteristic of nanocrystallites and nanoparticles, allowing the ferromagnetism even in oxides commonly not considered as magnetic materials.[23] Herewith the magnetic properties of α-Fe_2O_3 may also be enhanced after formation of iron oxide nanoparticles.[24]

Iron oxide films and nanostructures can be fabricated using different methods such as sputtering,[4,6,12,25,28] pulsed laser deposition,[7,10,26] molecular beam epitaxy,[9,27] electron beam evaporation,[5,28] microwave assisted hydrothermal[29] or solvothermal[35] processes, wet chemical method,[17] chemical vapor deposition (CVD),[31] spray pyrolysis,[14,32] and atomic layer deposition (ALD). ALD of iron oxide has been realized using $FeCl_3$ and H_2O,[2] $Fe(acac)_3$, i.e. $Fe(C_5H_7O_2)$, and O_2,[3] and $FeCp_2$ and O_3,[1,33–37] $FeCp_2$ and O_2,[38–41] $Fe_2(O^tBu)_6$ and H_2O,[33,42,43] $Fe(thd)_3$ and O_3,[44,45] as precursors. However, the body of literature reporting ALD of ferromagnetic-like materials verified by magnetometry is not yet large. For instance, recently a combination of liquid suspensions and ALD process has enabled growth of ferromagnetic nanotubes into anodized alumina.[36] Also in several other cases, Fe_2O_3 has been grown by ALD at rather low temperatures ranging from 140 to 200°C and/or on three-dimensional substrates (porous alumina, nanoparticles, carbon nanotubes)[1,33,34,39,41,43] which mostly necessitated the application of quite long precursor pulse times in the range of 20–720 s or long nitrogen purging times (25 s).[1,39,42] In most cases, the as-deposited films consisted of hematite Fe_2O_3 which was then reduced to the magnetite phase by post-deposition hydrogen treatment.[42,43] It is also to be noted, that magnetic tunnel junctions have already been created on the basis of CVD-processed Fe_2O_3/Fe_3O_4 and ALD-processed MgO.[46]

This study is devoted to the ALD of iron oxide films from a solid bis(cyclopentadienyl)iron, $FeCp_2$ (Cp = C_5H_5), and a liquid precursor (dimethylaminomethyl)ferrocene, $CpFeC_5H_4CHN(CH_3)_2$, novel in ALD. O_3 was used as an oxygen precursor. The aim of the study was the investigation of the effects of deposition temperature and MgO-doping on the phase composition and magnetization of the iron oxide based films.

Experimental

The films were grown in a commercial flow-type hot-wall reactor F120 (ASM Microchemistry, Ltd.)[47] on planar and three-dimensional

*Electrochemical Society Active Member.
[z]E-mail: kaupo.kukli@helsinki.fi

SiO_2/Si (aspect ratio 1:20) substrates using either ferrocene, $FeCp_2$ (Aldrich, 98%), or (dimethylaminomethyl)ferrocene, $CpFeC_5H_4CHN(CH_3)_2$ (Aldrich, 96%) and O_3 as precursors. For doping Fe_2O_3 with magnesium oxide, MgO was deposited using the ALD process based on $Mg(thd)_2$ (thd = 2,2,6,6-tetramethyl-3, 5-heptanedionato) and O_3[48] at the substrate temperature matching that suitable to iron oxide, i.e. above the ALD temperature window for MgO with the self-limiting growth. The films were grown with cycle times of < 2.5 s – 0.5 s – 2.0 s – 0.5 s for the sequence metal precursor pulse – purge – ozone pulse – purge. The cycle parameters were fixed in order to study the formation of ferric oxides on both planar and 3D substrates within reasonably short total deposition times. The films were grown from ferrocene in the substrate temperature range of 400–500°C, and from (dimethylaminomethyl)ferrocene in the range of 325–450°C. In the case of doping, the films were grown by alternating certain amounts of Fe_2O_3 and MgO binary cycles. For instance, the cycle sequence 100 × 1.5–0.5–2.0–0.5 s Fe_2O_3 + 4 × [3 × 1.0–0.5–1.5–0.5 s MgO + 100 × 1.5–0.5–2.0–0.5 s Fe_2O_3] means that after every 100 cycles of Fe_2O_3 three MgO deposition cycles were applied, four Fe_2O_3-MgO double layers were thus created. The relative amount of magnesium was varied by varying the ratio between MgO and Fe_2O_3 cycles. The number of MgO deposition cycles in each single layer was varied between 2 and 30 in the films later subjected to the magnetometry. Expectedly, such deposition recipes did not result in nanolaminates, but rather in doped films or mixtures, with crystallographic structures characteristic of iron oxides. In an additional experiment, nanolaminate-like structures of Fe_2O_3 and MgO layers were grown by alternate application of 100 or 150 cycles of MgO and 100 or 150 cycles of Fe_2O_3, repeated 8 or 5 times, respectively. Forming gas annealing (FGA) was carried out at 450°C for 30 min in N_2/H_2 (95%/5%) on both non-doped and doped samples, in order to induce (partial) reduction of Fe_2O_3 to Fe_3O_4.

The film structure was evaluated by grazing incidence X-ray diffraction (GIXRD) analysis performed using a PANalytical X'Pert PRO X-ray diffractometer with an incidence angle of 1 deg. Film thicknesses were measured by an Oxford INCA 350 energy dispersive X-ray (EDX) spectrometer connected to a Hitachi S-4800 scanning electron microscope (SEM). The EDX spectra were measured at 20 keV (The beam current and spectrometer gain were determined from a calibration measurement performed under the same beam conditions). The film thicknesses and metal ratios were calculated from the k ratios of Fe K_α and Mg K_α X-ray lines measured with the calibrated beam. The calculations were done with a GMRFILM program[49] assuming a density of 5.25 g/cm^3 for Fe_2O_3. SEM was exploited also for the visualization of the iron oxide surface morphology. Focused Ion Beam (FIB) milling with a FEI Quanta 3D 200i FIB/SEM instrument was used for making cross-sections of 3D trench structures. EDS mapping with an Oxford Instruments Xmax 50 mm^2 SSD detector in the FIB/SEM instrument was used for studying the film penetration into high aspect-ratio structures. A low 5 kV electron beam was used in order to improve the spatial resolution and light element sensitivity during the mapping of the elemental depth profiles.

The Fe_2O_3 films were evaluated also with Raman spectroscopy. The Raman spectra were recorded by using a Renishaw inVia micro-Raman spectrometer (spectral resolution 1.5 cm^{-1}). About 10 mW of the 514 nm line of an argon-ion laser was focused on sample through a 50× objective which also collects the backscattered Raman signal. The signal integration time was 30 s. A silicon reference sample was used for calibration of the Raman shift.

Soft X-ray absorption spectra (XAS) were measured on selected samples in total fluorescence yield (TFY) mode at beamline I511-3 in MAX-Lab (Lund, Sweden). The SX700 beamline monochromator resolution was set to 0.12 eV during the O 1s XAS measurements, and 0.19 eV for the Fe 2p XAS. The light was incident at 30 degrees with respect to the surface normal, and the detection direction was at approximately 10 degrees of the grazing exit angle, with the detector within the polarization plane. The monochromator energy scale calibration was checked against a Cr 2p reference spectrum. XAS was also measured using total electron yield (TEY) mode at beamline U49-2/PGM2 in Bessy-II (Berlin, Germany) with a spectral range of 85–1800 eV.[50,51] The plane gratings monochromator (PGM) resolution was set to 75 meV for the Fe 2p edge. The light was incident at 45 degrees with respect to surface normal. The TEY signal was detected using the drift current with a pico-amperometer (Keithley 486). Spectra were measured using 0.1 eV energy steps, the sampling time of each point was 0.1 s. The monochromator energy scale calibration was checked using the N 1s vibrational spectrum of N_2.

A selection of films was subjected to magnetic measurements. The measurements were performed using Vibrating Sample Magnetometer (VSM) option of the Physical Property Measurement System (PPMS) 14T (Quantum Design). Rectangular samples of dimensions 7 mm × 4 mm were fixed with GE vanish on the commercial quartz sample holders (Quantum Design). The temperature dependence of magnetization was perfomed in the temperature range of 10–350 K, and in presence of a magnetic field of 1000 Oe parallel to the film surface. Hysteresis measurements were performed by scanning the magnetic fields from −5 kOe to +5 kOe at temperatures selected in the range of 10–300 K. Diamagnetic signal arising from the silicon substrate was substracted from the general magnetization curve for all samples. The high temperature (300–1000 K) magnetization measurements were performed by VSM-Oven option for PPMS(Quantum Design) in order to determine the Curie temperature.

Results and Discussion

Growth and structure of iron oxide.— $FeCp_2$ did not enable efficient growth of the films below 400°C under the experimental conditions described above – the films remained highly profiled in thickness, i.e. nonuniform along the carrier gas flow direction. When using (dimethylaminomethyl)ferrocene, the deposition temperatures enabling better coverage of the surface with the film could be lowered by approximately 50 degrees. Already a visual inspection showed that the films grown from both precursors above 400°C were generally dark brown in color, non-transparent and possessed very rough surface. At temperatures lower than 400°C the films appeared bluish in color, more shiny and obviously smoother, possibly implying the increasing contribution from transparent half-metallic phases.

The processes using cyclopentadienyl-based iron precursors and O_3 are not to be regarded as the pure self-limiting ALD processes characterized by a growth rate saturating with the extension of the precursor pulse length, since the growth from $FeCp_2$ was intensified markedly with the increase in temperature.[52] The growth rate of Fe_2O_3 films deposited from $FeCp_2$ was 0.07–0.12 nm/cycle at 400°C.[52] The growth rate of the films deposited from $CpFeC_5H_4CHN(CH_3)_2$ was 0.14–0.15 nm/cycle at 375°C, increasing to 0.24, 0.33, and 0.70 nm/cycle at 400, 425 and 450°C, respectively. Thus, thermal decomposition of the cyclopentadienyl-based precursors is to be taken into account at the temperatures examined. The processes are, therefore, not to be regarded as pure ALD processes. Nevertheless, oxidation by using the ozone pulses was necessary in order to produce oxide films. At 350°C, the temperature was evidently too low for the efficient growth using such a short pulse times. Prolongation of the $CpFeC_5H_4CHN(CH_3)$ and O_3 pulses to 7.5 and 5 seconds, respectively, resulted in the growth of quite uniform films with the rate of 0.092 nm/cycle, though.

The formation of hematite and magnetite phases was mainly dependent on the deposition temperature and partially on the precursor chemistry. The non-doped as-deposited films grown at relatively high temperatures above 400°C consisted essentially of hematite, with some possible contribution from magnetite (and maghemite) especially in the films grown from (dimethylaminomethyl)ferrocene and/or after annealing. The films deposited from ferrocene at 500°C were identified to consist entirely of stable α-Fe_2O_3 (Fig. 1, upper panel). Such films remained dominantly hematite also after annealing as qualitative changes in the phase composition were not noticed. Although it is complicated to distinguish between XRD patterns of polycrystalline magnetite, maghemite and magnesioferrite, the reflections are denoted by the indexes attributed to magnetite for the

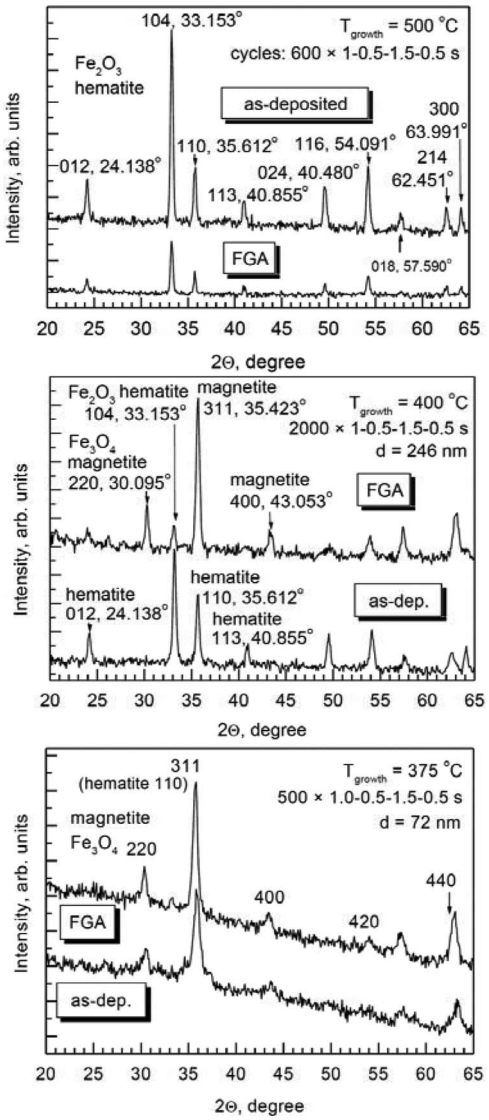

Figure 1. Grazing incidence X-ray diffraction patterns of iron oxide films grown at 500 and 400°C from $Fe(C_5H_5)_2$ (top and middle panels, respectively) and at 375°C from $CpFeC_5H_4CHN(CH_3)_2$ (bottom panel), Miller indexes are given for the peaks positioned in accord with the values in powder diffraction files of magnetite. Also the cycle sequences applied and film thicknesses are given by labels. The thickness of films grown at 500°C was ca. 120–150 nm, while the exact thickness determination occurred complicated due to the enhanced roughness and development of voids between grains.

reader's convenience and in order to stress the clear differences from hematite.

At relatively low temperature, 400°C, the as-deposited films were also consisting of hematite, without recognizable reflections from other phases (Fig. 1, middle panel). However, these films could partially be reduced to Fe_3O_4 after forming gas annealing. Further, at even lower temperatures, at which the films were already grown from (dimethylaminomethyl)ferrocene, the reflections in GIXRD patterns could all be attributed to the magnetite phase (Fig. 1, bottom panel), although the contribution from maghemite cannot be excluded. It is somewhat complicated to distinguish between some characteristic but closely located peaks, e.g. 311 and 110 reflections of magnetite, maghemite and hematite. It can also be noted that, when grown at 375°C, the films revealed a strong reflection at 35.4–35.6°, which became slightly shifted to lower angles after annealing, implying the reduction of hematite upon annealing.

According to the literature, hematite has earlier been formed e.g. in ALD of Fe_2O_3 from $FeCl_3$ and H_2O at 500°C.[2] Hematite was also formed in the ALD process based on $FeCp_2$ and O_3 at 200°C,[35] with essentially longer precursor pulse and purge times used compared to those applied in the present study. Increase in the process temperature has led to the formation of hematite instead of magnetite, as proven e.g. in studies on spray pyrolysis of iron oxide films.[25] Almost stoichiometric magnetite has been formed on silicon e.g. by PLD from Fe_3O_4 target at low oxygen pressure and temperature (483 K), whereas the increment in the deposition temperature to 558 and 683 K has slightly but gradually changed the stoichiometry of iron oxide toward hematite.[26] It can be noted, that on MgO, the PLD from Fe_2O_3 target has resulted in the formation of maghemite.[19] In another study, preferred growth of magnetite has been observed in a sputtering deposition process using relatively low sputtering power.[53] Maghemite and magnetite have actually been considered also as precursors for hematite, because hematite may be obtained from oxygen-deficient maghemite by calcination in air.[35] Transition from Fe_3O_4 to Fe_2O_3 has also been observed in a study devoted to the MOCVD of iron oxide, upon increasing the partial pressure of O_2 in the reactor.[31]

In our case, magnetite tended to form at relatively low growth temperatures, which in the first place can be due to the incomplete surface reactions. Possibly, at 375–400°C the rate of oxidation reaction was insufficient for the complete surface reaction and, thus, the oxygen-deficient phase Fe_3O_4 could form as an additive or, at the lowest temperatures, even as the dominant phase, although possibly mixed with maghemite. At 500°C, the surface reactions are fast enough to complete the oxidation during the rather short pulse times applied. The hematite phase formed is also structurally stable enough against reduction by hydrogen in forming gas during 30 min. Nevertheless, the forming gas has had considerable effect on the phase content of the films grown at lower temperatures, which refers to chemically less stable composition in these films or some less stable regions in the films, even if the as-deposited films mainly consisted of hematite according to GIXRD. In any case, the lowering of deposition temperature and, thus, approaching reaction threshold seems to have an effect to the composition at least as strong as the reduction by forming gas.

Doping with magnesium oxide.— The effect of MgO on the phase content was examined with the films grown in the temperature range of 375–425°C and mostly from the (dimethylaminomethyl)ferrocene. To clarify whether the phase content was mostly affected by the deposition temperature or by the inclusion of MgO, some films were specifically grown at 425°C (Fig. 2). At this temperature, non-doped as-deposited films completely consisted of hematite. After FGA, the films were, however, turned into magnetite giving characteristic 311, 220, 400 and 422 reflections with the weak but detectable shift between hematite 110 and magnetite 311 reflections (Fig. 2, upmost panel). Application of three MgO growth cycles between each 100 Fe_2O_3 cycles (MgO:Fe_2O_3 cycle ratio 3:100, Mg:Fe atomic ratio of 0.02 by EDX) resulted in the formation of mixed films containing both hematite and magnetite (Fig. 2, middle panel) which were again turned into magnetite/maghemite upon FGA. Further increment in the numbers of MgO cycles to 20 (Fig. 2, bottom panel) and 30 (not shown), giving Mg/Fe atomic ratios 0.23 and 0.38, respectively, resulted in the growth of films without unambiguous reflections of hematite at least after annealing, since the locations of the peaks were shifted toward those of magnetite/maghemite at lower 2*theta* values.

The reflections determined by GIXRD in this study coincide also with those attributed to magnetite in several other and very different works such as those describing the films or particles grown by sputtering,[18,53] pulsed laser deposition,[26] those describing the synthesis of powders under argon by using ammonium bases R_4NOH (R=CH_3, C_2H_5, C_3H_7) followed by hydrothermal treatment,[54] or those about materials obtained by oxidation of $Fe(OH)_2$ precipitate at low temperatures.[55]

One can question the presence of magnetite, since the reflections coincide with those of maghemite. The formation of solid solutions of maghemite and magnetite is highly likely. For instance, in an

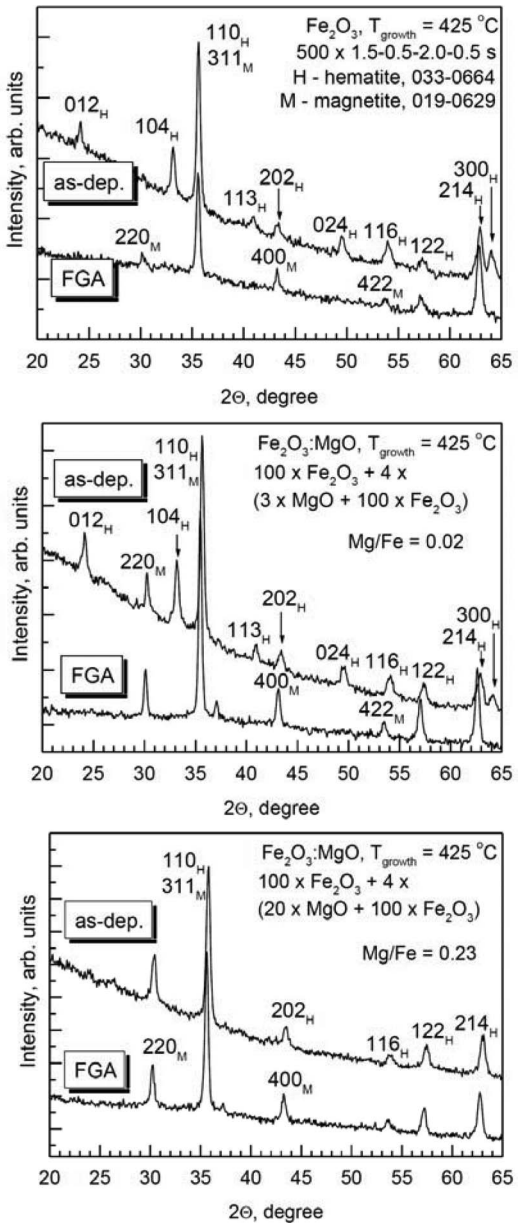

Figure 2. Grazing incidence X-ray diffraction patterns of iron oxide (top panel) and iron oxide- magnesium oxide (middle and bottom panels) films grown at 425°C from $Fe(C_5H_5)(C_5H_4CHN)(CH_3)_2$ in as-deposited and annealed (FGA) states. Miller indexes, growth cycle sequences, Mg to Fe atomic ratios, and PDF card numbers are given by labels.

earlier study devoted to a gas phase deposition of iron oxide, transition from maghemite to hematite was reported, occurring between 350 and 400°C.[56] In the latter study, the major peak appeared at ca. 30.5° and was attributed to the 220 reflection of γ-Fe_2O_3. Most of the other peaks were attributed to iron hydroxide, which do not match with the peaks observed in the present study, neither does the formation of hydroxides seem likely in the water-free process provided at that high temperature. Similarly, the peaks at 30.5 and 35.5° have been assigned as 220 and 311 of γ-Fe_2O_3 in a study on the iron oxide nanostructures obtained in a solvothermal process[30] as well as by a wet chemical method.[17] The presence of maghemite can thus be considered, although the main reflection, i.e. that at 26.103°, which could be significant while distinguishing between magnetite and maghemite, was not apparent in most of the patterns recorded in the present study as well as in the reference given. Traces of that peak (PDF card 039-1346) may be recognized in the iron oxide film as-deposited at 375°C (Fig. 1, bottom panel), and even in annealed film grown at 400°C (Fig. 1, middle panel). However, the appearance of the maghemite reflections was obviously not systematic in terms of growth or annealing parameters. Single phase maghemite could, in principle, be deposited on MgO substrate.[27] In addition, if the stoichiometry of the films were close to that of magnesioferrite $MgFe_2O_4$, then some significant peaks would also overlap with those of magnetite. For instance, locations of strong 220, 311 and 400 reflections of both $MgFe_2O_4$ (PDF card 017-0464)[57] and magnetite are identical. Distinction between maghemite, magnetite and magnesioferrite phases may be possible by XRD,[27] but remains complicated. However, the Mg/Fe atomic ratio measured here would not allow the formation of ternary phase as the major one but rather as a contributing additive.

The films deposited using thicker layers of constituent oxides, i.e with MgO:Fe_2O_3 cycle ratios 150:150 and 100:100 (Mg/Fe atomic ratios 0.39 and 0.59 for films with corresponding thicknesses 47 and 30 nm, respectively) were identified as layers crystallized already in the as-deposited state (not shown). The XRD patterns matched well with those of magnesioferrite (PDF card 017-0464). A double layer consisting of 8 nm thick MgO film and a 162 nm thick Fe_2O_3 film grown at 375°C was essentially a tetragonal maghemite (PDF card 025-1402). It is to be noted that MgO layers were not crystallized, because no reflections characteristic of MgO were detected. These films were, however, grown as reference samples for structural analysis, because high amounts of magnesium oxide did not enhance the magnetization.

Some films grown at 400 and 375°C were evaluated by Raman spectroscopy which might allow detection of phases not visible by GIXRD. Room-temperature Raman spectra of selected films are depicted in Figure 3. The bands are denoted in accord with Shebanova et al.[58] In the spectra, one could at first consider bands at 225, 293, 412, 498, 613, and 1320 cm^{-1} which are typical for α-Fe_2O_3, i.e. the hematite phase. Further, bands at 380, 500, 720, 1450 and 1580 cm^{-1} are typical of γ-Fe_2O_3 (maghemite) and the bands at 668, 538, 306, and 193 cm^{-1} are typical for Fe_3O_4 (magnetite).[58,59] It should also be mentioned, that the shoulder at 700 cm^{-1} for the main band at 668 cm^{-1} (Fig. 3, the 3rd panel) can also be attributed to magnesioferrite according to the Raman database. One could conclude that the non-doped films (not shown) as well as the lightly doped films (Fig. 3, top panel) grown at 400°C dominantly consisted of hematite. Weak bands at 538 and 668 cm^{-1}, characteristic of magnetite, were also present, though. In the film grown using MgO:Fe_2O_3 cycling ratio of 1:100 at 400°C, the relative significance of the magnetite bands was increased compared to the non-doped films, although Mg was not detected in the EDX spectra of those films. In the non-doped film grown at 375°C, the Raman spectra were changed, revealing the dominance of magnetite (not shown), with some implications from maghemite (720 cm^{-1}) as well as those of hematite (1320 cm^{-1}). However, the significances of both maghemite and hematite bands were decreased after annealing. Furthermore, in the films grown using MgO:Fe_2O_3 cycling ratio of 2:100 at 375°C (Mg/Fe atomic ratio of 0.017), the significance of the magnetite bands became stronger, especially that at 668 cm^{-1} (Fig. 3, middle panel). In this film, the relatively weaker decrease of the bands at around 1400 cm^{-1} after annealing just might be connected to the contribution of maghemite. In these kinds of films, formation of the magnesioferrite phase is also not to be excluded, based on the shoulder at 700 cm^{-1}. According to the Raman results, it seems that the films grown using MgO:Fe_2O_3 cycling ratio of 5:100 (Mg/Fe atomic ratio of ca. 0.05) at 425°C were a mixture of hematite and magnetite, whereas the films grown at 375°C mainly consisted of magnetite (Fig. 3, bottom panel). In the spectra, several peaks implied the presence of the maghemite phase. This phase was not clearly detected by GIXRD. Also, in the as-deposited films grown at 400°C, magnetite was not recognized by GIXRD, whereas Raman indicated the presence of the magnetite as an additional phase. In general the Raman results support the observations by GIXRD.

Also the XAS spectra of Fe 2p and O 1s (Fig. 4) align well with those measured earlier from the different iron oxides.[60–62] The Fe 2p spectra of the samples deposited at 400°C (Fig. 4a, b) are

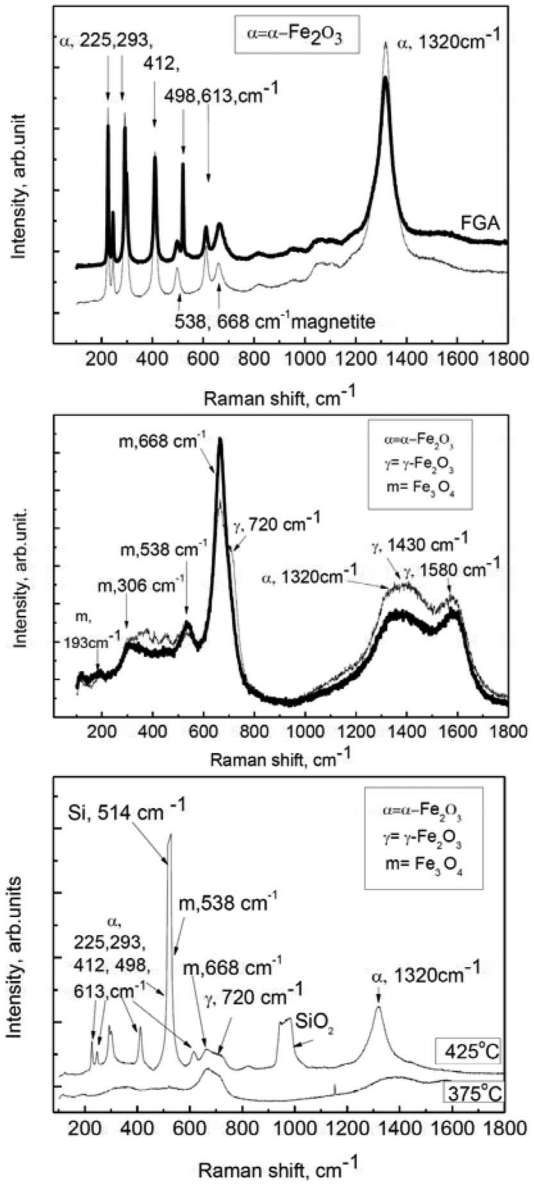

Figure 3. Raman spectra of 328 nm thick Mg-Fe oxide film (cycle ratio 1:100) grown at 400°C from $FeCp_2$ (top panel), 425 nm thick Mg-Fe oxide film (cycle ratio 2:100, Mg/Fe = 0.017) grown at 375°C from $CpFeC_5H_4CHN(CH_3)_2$ (middle panel), and those of 65 and 223 nm thick Mg-Fe oxide films grown with cycle ratio 5:100 (Mg/Fe = 0.05–0.06) at 425 and 375°C, respectively (bottom panel). Patterns taken from annealed films are bold and labeled with FGA.

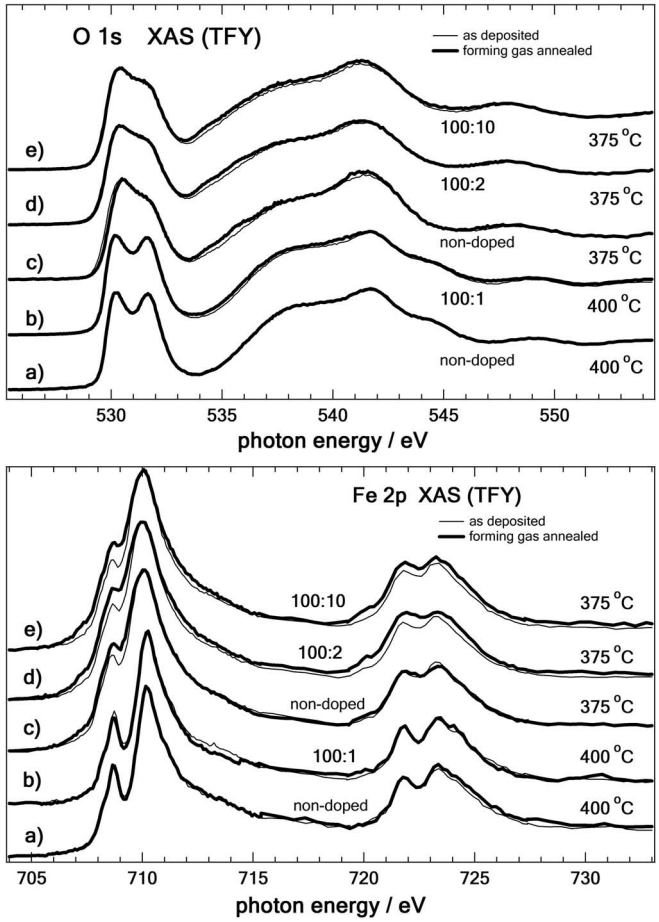

Figure 4. X-ray absorption spectra, measured in total fluorescence yield mode, of 117 nm thick non-doped film grown at 400°C from $FeCp_2$ (a), 328 nm thick film grown with Fe_2O_3:MgO cycle ratio 100:1 (no Mg detected) at 400°C from $FeCp_2$ (b), 72 nm thick non-doped film grown at 375°C from $CpFeC_5H_4CHN(CH_3)_2$ (c), 425 nm thick film grown with cycle ratio 100:2 (Mg/Fe = 0.017) at 375°C from $CpFeC_5H_4CHN(CH_3)_2$ (d), and 411 nm thick film grown with cycle ratio 100:10 (Mg/Fe = 0.062) at 375°C from $CpFeC_5H_4CHN(CH_3)_2$ (e). Fe L_3 edges are depicted in upper panel, while the O K-edge spectra are shown in lower panel.

characteristic of hematite with about 1.5 eV split and double-peak L_3 structure, whereas the spectra of the sample deposited at 375°C (Fig. 4c, d, e) resemble magnetite spectra, with the lower energy L_3 main peak at 709 eV only partly resolved and visible as a low energy shoulder of the L_3 maximum. As the main features of the hematite and magnetite L_3 XAS tend to overlap to a degree, Domashevskaya et al.[60] have noted that, when Fe^{2+} ions are present in the sample, the shoulder ca. 1–1.5 eV below the more prominent L_3 and the L_2 main peaks is increased. The intensities at these dinstinguishable positions in the spectra are indeed prominent also in our spectra, which also show closer resemblance to magnetite spectra according to the L_3 main features. The annealing (FGA) procedure further enhanced and shifted the smaller L_3 main peak slightly above 708.5 eV toward the main L_3 peak at 710 eV, so that the overall spectral curve became more similar to what has been observed for magnetite.[60] The measured O 1s XA spectra agree well with the trends indicated by the Fe 2p spectra and give additional support to the proposition that magnetite is indeed present and dominant in the samples deposited at 375°C from $CpFeC_5H_4CHN(CH_3)_2$. It is also to be mentioned that the film deposited with low amount of MgO cycles (ratio 100:1) resembles hematite according to the Fe 2p spectra and magnetite according to the O 1 s spectra (Fig. 4).

XAS measurements with TEY at Fe 2p (Fig. 5) edge were used to characterize pure and Mg-doped Fe_2O_3 films grown at 425°C with (dimethylaminomethyl)ferrocene, described by XRD (Fig. 2), SEM (Fig. 6) and Table II. Similarly to the samples measured with TFY, the undoped Fe_2O_3 samples and those doped with 0.02 at.% Mg resembled the hematite spectrum, while samples with increased doping level (0.2 at.% and 0.4 at.%) showed a decreased intensity of the shoulder at 708.5 eV in the Fe 2p spectrum, possibly due to the presence of a small magnetite component in agreement with the XRD data.

Morphology.— The growth temperature, film thickness and MgO doping level influenced the film morphology. Figure 6 demonstrates the SEM images taken from non-doped and doped films grown at 425°C from (dimethylaminomethyl)ferrocene.

One can see that the non-doped films tended to be extremely rough when grown to markedly high thicknesses and/or at temperatures above 400°C (Fig. 6, upmost panel). This is valid also for

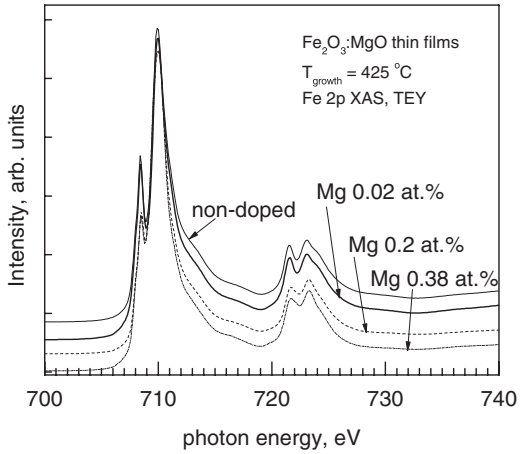

Figure 5. X-ray absorption spectra, measured in total electron yield mode, of non-doped and doped films grown at 425°C from $CpFeC_5H_4CHN(CH_3)_2$. The legend indicates the magnesium (oxide) content in the films measured by EDX.

the films grown using ferrocene (not shown). Such films consisted of columns, grains or pillars formed, possibly, on continuous base layer with large voids between the pillars. Already small amounts of magnesium oxide (Mg/Fe = 0.02) caused some increase in the density of the pillars/grains and decrease in the width of the voids (Fig. 6, 2nd panel from top). Further increase in the relative amount of MgO resulted in the formation of quite continuous film surfaces and also smoothening of the film surface visible even by naked eye, as mentioned above. Moreover, the addition of MgO also had a marked effect on the film thickness. Application of quite low amounts of MgO enhanced the growth resulting in higher total thickness of the films. Increment in the number of MgO deposition cycles, on the other hand, reduced the film growth rate. For instance, using $MgO:Fe_2O_3$ cycle ratio of 20:100 resulted in films with thickness nearly two times lower than that of non-doped Fe_2O_3 films. The surfaces of the films grown to thicknesses below 70–80 nm at temperatures below 400°C remained smoother without no particular features which could indicate the formation of separated columns or large grains on the surface (not shown).

Fig. 7 represents cross-sectional SEM and EDX mapping images taken from an iron oxide film deposited on 3D substrates. One can conclude, that the films could be grown conformally into trenches with aspect ratio 1:20 using the same cycle time parameters as those applied for the growth on planar substrates. EDX allowed one to detect signals from iron along with the depth of the trenches, including the bottom area. Distribution of oxygen could be mapped as well.

Magnetometry.— Magnetic properties of non-doped films.—Magnetization vs. magnetic field measurements revealed that the as deposited and annealed films both exhibit saturated hysteresis loops at room temperature, while magnetization was found to be enhanced in films annealed in hydrogen. Coercivity, H_C, and saturation magnetization, μ_S, determined from the hysteresis curves expectedly tended to increase with the decrease in measurement temperature. No systematic dependences of both H_C and μ_S on the film thickness were observed, though.

The films grown at high temperatures, 500°C, from ferrocene were defined consisting completely of hematite, as described above. These films possessed μ_S as low as 20 emu/cm^3 in as-deposited state and no measurable H_C (not shown). After FGA, the magnetization-versus-field (***M-H***) curves (not shown) demonstrated that μ_S increased by approximately an order of magnitude and H_C was measurable up to 500 Oe at room temperature. This means that although no phase changes were noticed upon annealing by GIXRD (Fig. 1), some weak reduction must have been occurred. The rest of the samples magnetically characterized were grown at temperatures lower than 500°C. Magnetic parameters for selected films are given in Table I.

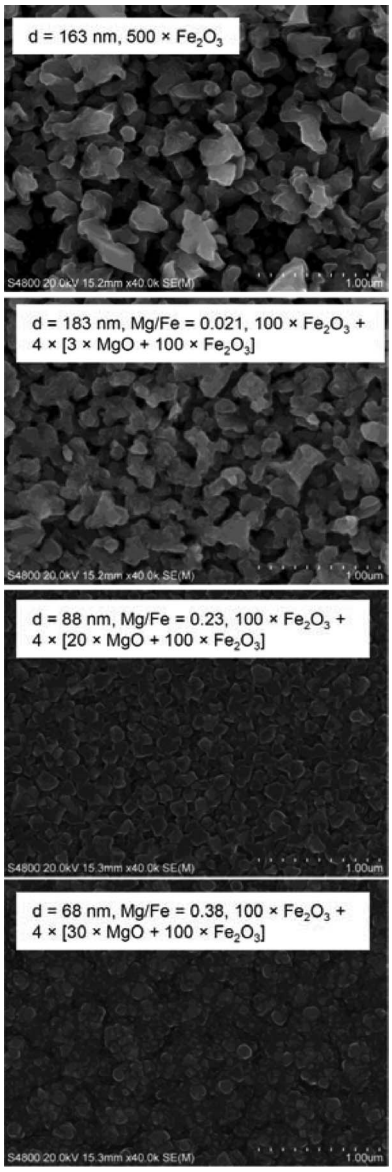

Figure 6. Bird-eye scanning electron microscopy images of Fe_2O_3 (topmost panel) and Fe_3O_4-MgO films (2nd to 4th panel from top) grown using different cycle sequences indicated by labels. The films were grown from $CpFeC_5H_4CHN(CH_3)_2$ at 425°C. Film thicknesses and Mg to Fe atomic ratios are also given by labels.

For instance, in a 246 nm thick film grown at 400°C from ferrocene, consisting of hematite (Fig. 1), μ_S remained rather low, just reaching 62 emu/cm^3 at room temperature. After FGA, μ_S was increased several times, reaching 360 emu/cm^3. It is to be mentioned, that the μ_S was weakly dependent on the measurement temperature in all samples in this study, whereas H_C varied noticeably at temperatures ranging from 10 to 300 K, naturally increasing with the decrease in the measurement temperature. For instance, the H_C in the sample as-deposited at 400°C was 300 Oe at room temperature, increasing to 600 and 780 Oe at 100 and 10 K, respectively. Annealing caused reduction in H_C to 135, 230 and 380 Oe at 300, 100 and 10 K, respectively. The decrement in the H_C upon annealing may be explained by the crystal growth and accompanying increase in the average domain size in the films. The inverse correlation sometimes noticed between film thickness and magnetization characteristics may also support the importance of the crystallite size.

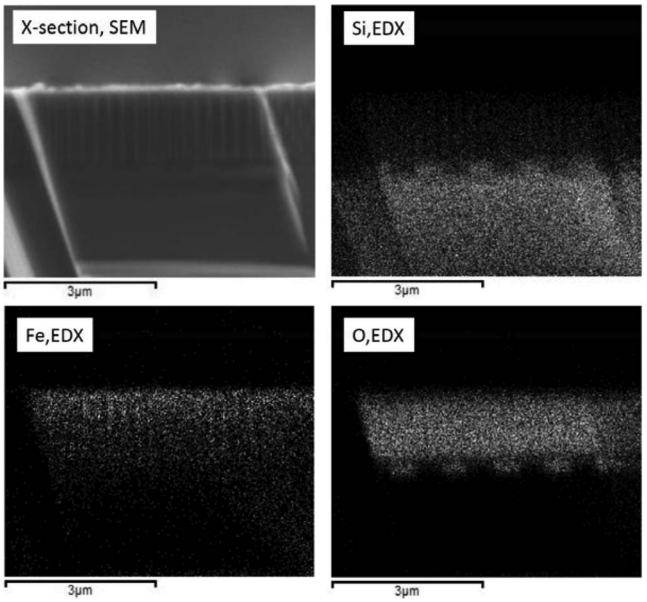

Figure 7. Cross section SEM/EDX images from a 72 nm thick film grown from $CpFeC_5H_4CHN(CH_3)_2$ at 375°C usin 500 ALD cycles on 3D substrates. The elements detected are denoted by labels.

It was actually observed (not shown) that films demonstrating defined magnetic properties could be grown at temperatures as low as 350°C, although the films were already quite non-uniform in thickness as well as magnetization level.

Magnetometry on magnesium oxide-doped films.—In the films deposited using the Fe_2O_3:MgO cycle ratio of 100:1, magnesium could not be detected by EDX. However, already Raman and XAS spectra have indicated an increased contribution from magnetite in the low-doped films as was described above. A 328 nm thick film deposited using the cycle ratio 100:1 at 400°C was morphologically already different and somewhat smoother compared to a 246 nm thick Fe_2O_3 film grown at the same temperature (Fig. 6). The doped film possessed H_C values of 480, 500 and 810 Oe at 300, 100 and 10 K in as-deposited state, and, correspondingly, 410, 410 and 750 Oe after annealed. The μ_S was 222–228 and 206–217 emu/cm^3 in the as-deposited and annealed films, respectively. Thus, both H_C and μ_S were increased after adding a minor amount of MgO pulses.

The films grown from $CpFeC_5H_4CHN(CH_3)_2$ at 425°C (XRD results in Fig. 2) also possessed magnetic properties influenced by MgO. Comparing the non-doped 163 nm thick Fe_2O_3 with lightly doped 183 nm thick sample (Table II), one could detect noticeable increase in μ_S upon adding MgO, whereas the coercivities remained comparable. Both H_C and μ_S expectedly increased after annealing. Further, after stronger doping (Mg/Fe = 0.23 and 0.38) the coercivities still remained quite comparable, but μ_S was dropped markedly. The effect of annealing remained the same. Drop in the μ_S might partially be explained by the drop in the film growth rate and, consequently, reduced thickness and, partially, by the possible formation of magnesium-rich phase, magnesioferrite, in addition to magnetite/maghemite. In any case, it seems that, at elevated substrate temperatures, it would be useful to keep the Mg content as low as possible, below Mg to Fe ratio of 0.1, in order to get smooth films and stronger magnetization.

The films grown from $CpFeC_5H_4CHN(CH_3)_2$ at 375°C also demonstrated properties influenced by MgO-doping (Fig. 8). The H_C tended to decrease upon the increase in the Mg content. In the non-doped and as-deposited films the H_C ranged from 485 to 1950 Oe between 300 and 10 K (not shown). In the films with Mg/Fe atomic ratio of 0.017 the H_C was in the range of 300–1260 Oe between 300 and 10 K. Upon further increase in the Mg content to Mg/Fe ratio of 0.062 the H_C was decreased, being in the range of 150–460 Oe between 300 and 10 K (Fig. 8). The annealing procedure again decreased the H_C (Fig. 8). On the other hand, μ_S was increased with the Mg content up to a certain limit. One could see that high amounts of magnesium may not be advantageous in terms of increasing both H_C and μ_S, maybe due to the formation of an additive ternary phase, e.g. magnesioferrite, in the film bulk.

Curie temperatures (ferro-/ferri-paramagnetic transitions) were found to be in the range of 820–895 K, determined from zero-field-cooled high temperature magnetization curves. The Curie temperatures were not systematically dependent on the iron precursor used, growth temperature and not even noticeably on the film composition, varying between 820 and 895 K. The Curie temperature of magnetite and Néel temperature of hematite bulk materials are about 850 and

Table I. Precursors, growth temperatures (T_{growth}), thicknesses, compositions (Mg/Fe), coercitivities (H_C), saturation magnetization values (μ_C) and Curie temperatures (T_C) of some representative films investigated in this study.

					H_C, O_e			μ_S, emu/cm^3			
precursors	T_{growth}	thickness	Mg/Fe ratio by EDX	state	300 K	100 K	10 K	300 K	100 K	10 K	T_C,K
$FeCp_2NMe_2$	450°C	705 nm	–	as-dep	425	900	1175	104	107	107	870
				FGA	330	750	800	375	372	370	860
$FeCp_2$	400°C	246 nm	–	as-dep	300	600	780	62	64	65	860
				FGA	135	230	250	360	381	386	895
$FeCp_2NMe_2$	375°C	262 nm	–	as-dep	485	1200	1950	193	205	206	850
				FGA	325	500	850	346	356	359	840
$FeCp_2NMe_2$, $Mg(thd)_2$	375°C	425 nm	0.017	as-dep	300	830	1260	200	207	209	845
				FGA	260	310	580	280	282	283	840
$FeCp_2NMe_2$, $Mg(thd)_2$	375°C	411 nm	0.062	as-dep	150	330	460	491	496	497	830
				FGA	200	210	380	274	289	291	820

Table II. Growth cycle sequences, thicknesses, Mg/Fe ratios, coercivities, and saturation magnetization values of doped films grown at 425°C, measured at room temperature. The deposition cycle times were 1.0–0.5–2.0–0.5 s.

Cycle sequencing	thickness, nm	Mg/Fe ratio	H_C, Oe as-dep.	H_C, Oe FGA	μ_S, emu/cm^3 as-dep.	μ_S, emu/cm^3 FGA
$500 \times Fe_2O_3$	163	0	200	340	217	344
$100 \times Fe_2O_3 + 4 \times [3 \times MgO + 100 \times Fe_2O_3]$	183	0.021	180	360	260	496
$100 \times Fe_2O_3 + 4 \times [20 \times MgO + 100 \times Fe_2O_3]$	88	0.23	170	420	224	220
$100 \times Fe_2O_3 + 4 \times [30 \times MgO + 100 \times Fe_2O_3]$	68	0.38	235	330	193	391

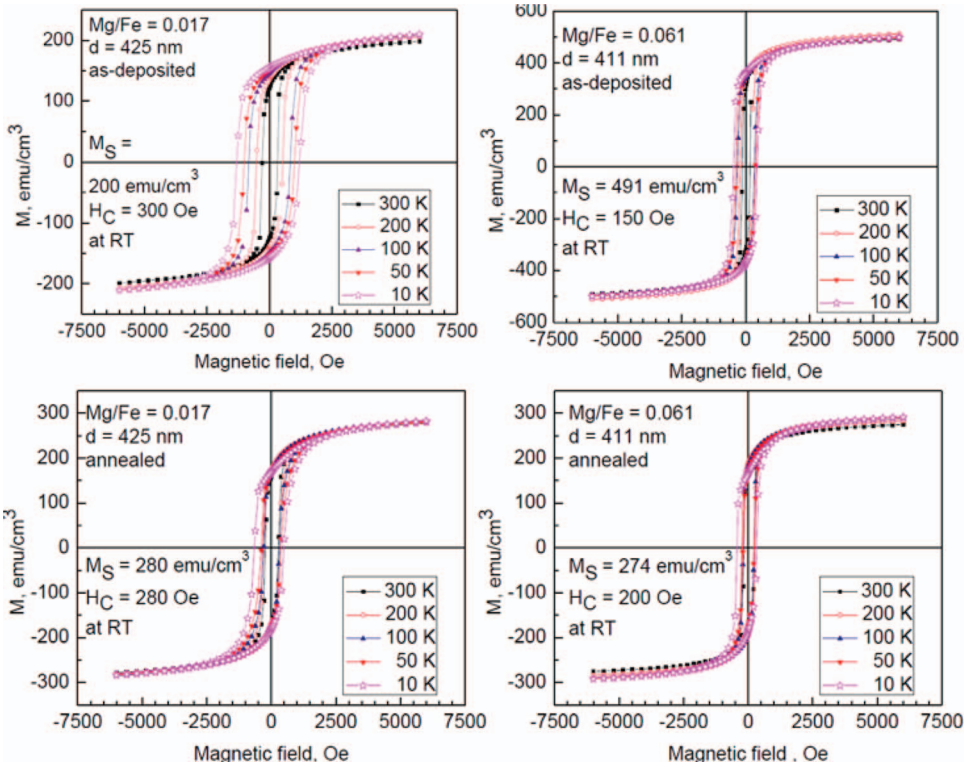

Figure 8. Representative magnetization *versus* external field curves of doped iron oxide films deposited from $CpFeC_5H_4CHN(CH_3)_2$ at 375°C. Mg/Fe atomic ratios, film thicknesses, hysteresis parameters and measurement temperatures are given by labels. Annealing was carried out in forming gas at 450°C for 30 min. (Color online)

950 K, respectively.[16] Most of the films measured in the present work demonstrated Curie temperatures close to 850 K, being indicative of the significance of reduced oxide. In any case the Curie temperatures determined were in line with those of iron oxide.

Zierold et al.[36] have observed in their iron oxide films reduced to magnetite (Fe_3O_4) a low-temperature transformation, i.e. jump in magnetization-versus-temperature curves known as the Verwey transition. At the Verwey transition temperature, T_V, ca. 120 K, magnetite is supposed to transform from cubic ($T > T_V$) to monoclinic ($T < T_V$) symmetry. This transformation is related to changes in cation ordering and, at a slightly higher temperature (ca. 130 K) to changes in magnetocrystalline anisotropy as well as switching the easy and hard magnetization axes. The Verwey transition can be used for identification of magnetite in pure or mixed phase samples. In our films, Verwey transition could be considered in some nondoped and slightly magnesium-doped samples after annealing in forming gas (Fig. 9). The transition lost its prominence in as-deposited films, in relatively disordered films grown at the lowest temperatures examined and in films containing relatively higher amounts of magnesium oxide. Nevertheless, the jumps in the M-T curves observed at around 120–125 K may well indicate the presence of magnetite in our samples.

Reduction of film thickness.—Thinner films grown in parallel on planar and into 3D (Fig. 7) substrates demonstrated clearly measurable magnetic properties (not shown). These films behaved generally in the same way as thicker films in terms of ***M-H*** curves. A non-doped 72 nm thick iron oxide possessed, in the as-deposited state, coercivities of 960 and 1350 Oe at 300 and 10 K, respectively. After FGA, the values were decreased to 380 Oe at 300 K and increased to 1700 Oe at 10 K. Saturation magnetization was 158–205 emu/cm^3 in the as-deposited state and increased to 224–242 emu/cm^3 after FGA. Also, μ_S slightly increased with the decrease in the measurement temperature. Further, after low doping of iron oxide with MgO (MgO/Fe_2O_3 cycle ratio of 2:100) a 47 nm thick film was grown, in which the Mg was not determined by EDX probably due to the low film thickness. H_C remained noticeably lower, 190 and 270 Oe, in as-deposited and annealed states compared to those in non-doped oxide. Magnetization was somewhat increased in doped films in as-deposited state to 217 emu/cm^3, but remained lower, 60 emu/cm^3, after annealing. After further increase in Mg/Fe ratio to 0.043 in a film grown to thickness of 59 nm with cycle ratio of 5:100, the H_C was even more decreased. The measured values in the as-deposited films were 140 and 1250 Oe at 300 and 10 K, respectively, and 280 and 950 Oe in the annealed films. The μ_S values were decreased to 60–65 emu/cm^3 in the as-deposited films, and were increased to 190–200 emu/cm^3 after FGA. Curie temperatures in all these films were between 840 and 850 K. The optimization of the film composition and thickness would need more detailed process parametrization in the future studies.

Both Raman and XAS measurements in the present study have revealed features characteristic of magnetite whereas at least Raman also referred to the maghemite. The films grown in this study at elevated temperatures, and consisting of hematite, did not exhibit enhanced magnetization, though.

Summary

Fe_2O_3/Fe_3O_4 films were grown by atomic layer deposition on planar and three-dimensional SiO_2/Si substrates using $FeCp_2$ and $CpFeC_5H_4CHN(CH_3)_2$, as metal precursors, and O_3 as oxygen precursor in the substrate temperature range of 350–500°C. The precursor pulse and purge times were kept below 2.5 seconds. Application of $FeCp_2$ enabled reliable formation of the films at 400°C and higher temperatures, whereas $CpFeC_5H_4CHN(CH_3)_2$ allowed the reduction of the growth temperature by about 50 degrees. The films deposited at 450–500°C consisted of major hematite phase, whereas in the films grown at 375–400°C the formation of magnetite or maghemite became more likely. Several films were annealed in forming gas in order to study the possibility to partially reduce the hematite and give rise to the formation of magnetite. The significance of the reduction increased with the decrease in the deposition temperature.

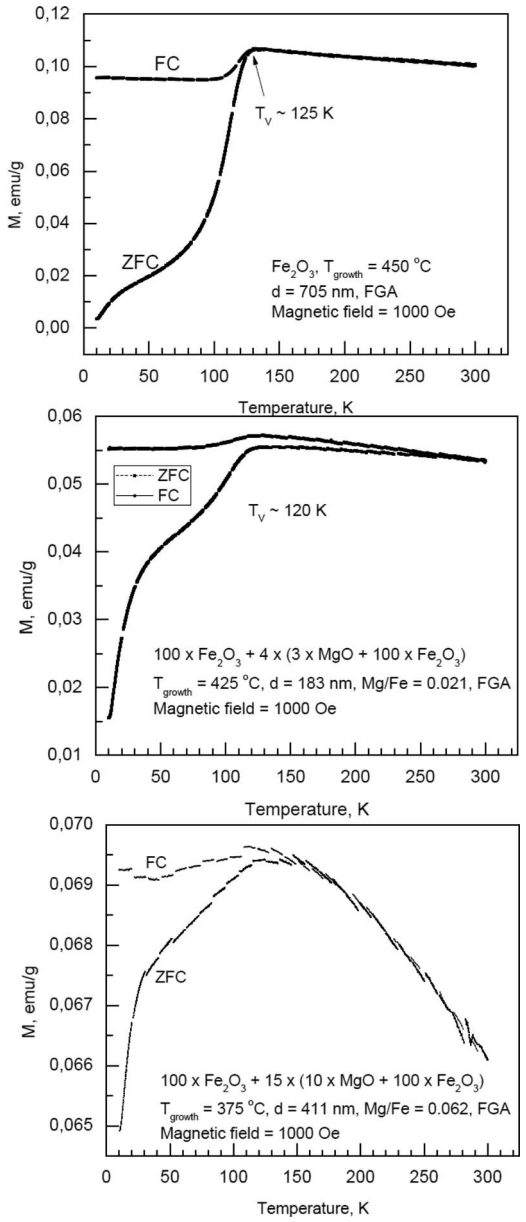

Figure 9. Magnetization versus measurement temperature curves of selected samples after forming gas annealing measured under zero field cooling (ZFC) and field cooling (FC) regimes. The composition, growth temperatures and film thicknesses are described by labels. The peaks associated with the Verwey transition of magnetite are denoted by T_V.

Several films were also mixed or doped by MgO, also grown by ALD from $Mg(thd)_2$. The Mg/Fe atomic ratio was varied between 0.0017 and 0.38. MgO affected the structure of the host material, increasing the probability of the formation of magnetite, which was most clearly proven in the films grown at 425°C, i.e. at a temperature at which the hematite was still formed as the major phase in the as-deposited non-doped films.

Both non-doped and doped films showed ferro- or ferrimagnetic properties. Coercivity up to 960 Oe and saturation magnetization up to 496 emu/cm^3 were achieved at room temperature in the as-deposited Fe_2O_3/Fe_3O_4 and Fe_2O_3/Fe_3O_4-MgO films. The coercivity generally decreased and magnetization was increased after annealing. The effect was the clearest in the films doped lightly with MgO, i.e. at Mg/Fe ratios below 0.02. High amounts of magnesium were not advantageous for either coercivity or magnetization, presumably due to the formation of additional ternary phases in the film bulk.

Acknowledgments

Dr. Petr Brazda is acknowledged for critical reading the manuscript. The work was partially supported by Finnish Center of Excellence in Atomic Layer Deposition (Academy of Finland), Estonian Ministry of Education and Research (targeted projects SF0180042s07 and SF0690029s09), Estonian Science Foundation (grant no. ETF8440), Estonian Center of Excellence in Research Project TK117T "High-technology Materials for Sustainable Development", and the European Community - Research Infrastructure Action under the FP6 Structuring the European Research Area Program (through the Integrated Infrastructure Initiative Integrating Activity on Synchrotron and Free Electron Laser Science)

References

1. B. M. Klahr, A. B. F. Martinson, and T. W. Hamann, *Langmuir*, **27**, 461 (2011).
2. M. Aronniemi, J. Saino, and J. Lahtinen, *Thin Solid Films*, **516**, 6110 (2008).
3. M. de Ridder, P. C. van de Ven, R. G. van Welzenis, H. H. Brongersma, S. Helfensteyn, C. Creemers, P. Van Der Voort, M. Baltes, M. Mathieu, and E. F. Vansant, *J. Phys. Chem., B*, **106**, 13146 (2002).
4. M. B. Yazdi, M.-L. Goyallon, T. Bitsch, A. Kastner, M. Schlott, and L. Alff, *Thin Solid Films*, **519**, 2531 (2011).
5. S. Jain, A. O. Adeyey, and D. Y. Dai, *J. Appl. Phys.*, **95**, 7237 (2004).
6. C. Park, Y. Peng, J.-G. Zhu, D. E. Laughlin, and R. M. White, *J. Appl. Phys.*, **97**, 10C303 (2005).
7. T. Tepper, F. Ilievski, C. A. Rossa, T. R. Zaman, R. J. Ram, S. Y. Sung, and B. J. H. Stadler, *J. Appl. Phys.*, **93**, 6948 (2003).
8. J. Ma, J. Hu, Z. Li, and C.-W. Nan, *Adv. Mater.*, **23**, 1062 (2011).
9. P. J. van der Zaag, P. J. H. Bloemen, J. M. Gaines, R. M. Wolf, P. A. A. van der Heijden, R. J. M. van de Veerdonk, and W. J. M. de Jonge, *J. Magn. Magn. Mater.*, **211**, 301 (2000).
10. J. Orna, L. Morellon, P. A. Algarabel, J. A. Pardo, S. Sangiao, C. Magen, E. Snoeck, J. M. De Teresa, and M. R. Ibarra, *IEEE Transact Magn.*, **44**, 2862 (2008).
11. R. Arras, L. Calmels, and B. Warot-Fonrose, *J. Phys.: Conf. Ser.*, **200**, 072008 (2010).
12. P. Li, E. Y. Jiang, and H. L. Bai, *J. Phys. D: Appl. Phys.*, **44**, 075003 (2011).
13. A. Zolotaryov, J. Bachmann, J. M. Montero-Moreno, K. Pitzschel, and K. Nielsch, *Precision Eng.*, **35**, 496 (2011).
14. W. B. Ingler Jr. and S. U. M. Khan, *Thin Solid Films* **461**, 301 (2004).
15. R. K. Kotnala, J. Shah, M. C. Mathpal, K. C. Verma, S. Singh, and S. Lovkush, *Thin Solid Films*, **519**, 6135 (2011).
16. G. Pullaiah, E. Irving, K. L. Buchan, and D. J. Dunlop, *Earth Planet. Sci. Lett.*, **28**, 133 (1975).
17. E. Darezereshki, *Mater. Lett.*, **65**, 642 (2011).
18. X. Tang, H. Zhang, H. Su, Z. Zhong, and Y. Jing, *Trans. Nonferrous Met. Soc. China*, **16**, s249 (2006).
19. T. Tepper and C. A. Ross, *J. Appl. Phys.*, **91**, 4453 (2002).
20. R. J. Willey, S. A. Oliver, G. Oliveri, and G. Busca, *J. Mater. Res.*, **8**, 1418 (1996).
21. S. Da Dalt, A. S. Takimi, V. C. Sousa, and C. P. Bergmann, *Particulate Sci. Tech.: Int. J.*, **27**, 519 (2009).
22. R. J. Harrison and A. Putnis, *Surv. Geophys.*, **19**, 461 (1999).
23. A. Sundaresan and C. N. R. Rao, *Nano Today*, **4**, 96 (2009).
24. M. Tadić, D. Marković, V. Spasojević, V. Kusigerski, M. Remškar, J. Pirnat, and Z. Jagličić, *J. Alloys Compd.*, **441**, 291 (2007).
25. D. T. Margulies, F. T. Parker, F. E. Spada, R. S. Goldman, J. Li, R. Sinclair, and A. E. Berkowitz, *Phys. Rev., B*, **53**, 9175 (1996).
26. M. L. Paramês, J. Mariano, Z. Viskadourakis, N. Popovici, M. S. Rogalski, J. Giapintzakis, and O. Conde, *Appl. Surf. Sci.*, **252**, 4610 (2006).
27. S. Thevuthasan, D. E. McCready, W. Jiang, S. I. Yi, S. Maheswaran, K. D. Keefer, and S. A. Chambers, *Nucl. Instr. Meth. Phys. Res., B*, **161–163**, 510 (2000).
28. D. Tripathy, A. O. Adeyeye, and C. B. Boothroyd, *J. Appl. Phys.*, **99**, 081105 (2006).
29. X. Hu, J. C. Yu, J. Gong, Q. Li, and G. Li, *Adv. Mater.*, **19**, 2324 (2007).
30. S.-W. Cao, Y.-J. Zhu, and Y.-P. Zeng, *J. Magn. Magn. Mater.*, **321**, 3057 (2009).
31. S. Dhar, K. Shalini, and S. A. Shivashankar, *Bull. Mater. Sci.*, **31**, 723 (2008).
32. R. N. Goyal, D. Kaurb, and A. K. Pandey, *Mater. Chem. Phys.*, **116**, 638 (2009).
33. J. Escrig, J. Bachmann, J. Jing, M. Daub, D. Altbir, and K. Nielsch, *Phys. Rev., B*, **77**, 214421 (2008).
34. J. Bachmann, J. Escrig, K. Pitzschel, J. M. M. Moreno, J. Jing, D. Görlitz, D. Altbir, and K. Nielsch, *J. Appl. Phys.*, **105**, 07B521 (2009).
35. A. B. F. Martinson, M. J. DeVries, J. A. Libera, S. T. Christensen, J. T. Hupp, M. J. Pellin, and J. W. Elam, *J. Phys. Chem., C*, **115**, 4333 (2011).
36. R. Zierold, Z. Y. Wu, J. Biskupek, U. Kaiser, J. Bachmann, C. E. Krill, and K. Nielsch, *Adv. Funct. Mater.*, **21**, 226 (2011).
37. J. Gemmer, Y. Hinrichsen, A. Abel, and J. Bachmann, *J. Catalysis*, **290**, 220 (2012).
38. M. Rooth, A. Johansson, K. Kukli, J. Aarik, M. Boman, and A. Hårsta, *Chem. Vap. Deposition*, **14**, 67 (2008).
39. J. R. Scheffe, A. Francés, D. M. King, X. Liang, B. A. Branch, A. S. Cavanagh, S. M. George, and A. W. Weimer, *Thin Solid Films*, **517**, 1874 (2009).
40. J. R. Scheffe, M. D. Allendorf, E. N. Coker, B. W. Jacobs, A. H. McDaniel, and A. W. Weimer, *Chem. Mater.*, **23**, 2030 (2011).

41. X. Meng, M. Ionescu, M. N. Banis, Y. Zhong, H. Liu, Y. Zhang, S. Sun, R. Li, and X. Sun, *J. Nanopart. Res.*, **13**, 1207 (2011).
42. J. Bachmann, J. Jing, M. Knez, S. Barth, H. Shen, S. Mathur, U. Gösele, and K. Nielsch, *J. Am. Chem. Soc.*, **129**, 9554 (2007).
43. K. Pitzschel, J. M. M. Moreno, J. Escrig, O. Albrecht, K. Nielsch, and J. Bachmann, *ACS Nano*, **3**, 3463 (2009).
44. O. Nilsen, M. Lie, S. Foss, H. Fjellvåg, and A. Kjekshus, *Appl. Surf. Sci.*, **227**, 40 (2004).
45. M. Lie, H. Fjellvåg, and A. Kjekshus, *Thin Solid Films.*, **488**, 74 (2005).
46. R. Mantovan, M. Georgieva, M. Perego, H. L. Lu, S. Cocco, A. Zenkevich, G. Scarel, and M. Fanciulli, *Act. Phys. Pol., A*, **112**, 1271 (2007).
47. T. Suntola, *Thin Solid Films*, **216**, 84 (1992).
48. M. Putkonen, L.-S. Johansson, E. Rauhala, and L. Niinistö, *J. Mater. Chem.*, **9**, 2449 (1999).
49. R. A. Waldo, *Microbeam Analysis*, San Francisco Press, San Francisco, CA, p. 310 (1988).
50. D. Schmeisser, P. Hoffmann, and G. Beuckert, *Materials for Information Technology, Devices, Interconnects and Packaging, Engineering Materials and Processes*; Springer: New York, 2005.
51. M. Tallarida and D. Schmeisser, *Semicond. Sci. Technol.*, **27**, 074010 (2012).
52. A. Tamm, M. C. Dimri, J. Kozlova, A. Aidla, T. Tätte, T. Arroval, U. Mäeorg, H. Mändar, R. Stern, and K. Kukli, *J. Cryst. Growth*, **343**, 21 (2012).
53. Y. Peng, C. Park, and D. E. Laughlin, *J. Appl. Phys.*, **93**, 7957 (2003).
54. J. S. Salazar, L. Perez, O. de Abril, L. T. Phuoc, D. Ihiawakrim, M. Vazquez, J.-M. Greneche, S. Begin-Colin, and G. Pourroy, *Chem. Mater.*, **23**, 1379 (2011).
55. J. Wang, T. Deng, and Y. Dai, *J. Alloys Compd.*, **390**, 127 (2005).
56. M. Aronniemi, J. Lahtinen, and P. Hautojärvi, *Surf. Interface Anal.*, **36**, 1004 (2004).
57. R. S. de Biasi, L. H. G. Cardoso, J. B. De Campos, D. R. Sanchez, and J. B. M. da Cunha, *Mater. Res.*, **12**, 225 (2009).
58. O. N. Shebanova and P. Lazor, *J. Solid State Chem.*, **174**, 424 (2003).
59. A. M. Jubb and H. C. Allen, *Appl. Mater. Interfaces*, **2**, 2804 (2010).
60. E. P. Domashevskaya, S. A. Storozhilov, S. Yu, V. M. Turishchev, V. A. Kashkarov, O. V. Terekhov, Yu. Stognei, E. Kalinin, A. V. Sitnikov, and S. L. Molodtsov, *Bull. Russ. Acad. Sci.: Phys.*, **72**, 448 (2008).
61. A. Yamasaki, H. Kobori, H. Osawa, T. Nakamura, and A. Sugimura, *J. Phys.*, **150**, 042235 (2009).
62. C. K. Yang, J. W. Chiou, H. M. Tsai, C. W. Pao, J. C. Jan, S. C. Ray, C. L. Yeh, K. C. Huang, H. C. Hsueh, W. F. Ponga, M.-H. Tsai, H. H. Hsieh, H. J. Lin, T. Y. Hou, and J. H. Hsu, *Appl. Phys. Lett.*, **86**, 062504 (2005).